Shape-programmable magnetic soft matter

Guo Zhan Lum[a,b,c,1], Zhou Ye[a,1], Xiaoguang Dong[a,b,1], Hamid Marvi[d], Onder Erin[a,b], Wenqi Hu[a], and Metin Sitti[a,b,2]

[a]Physical Intelligence Department, Max Planck Institute for Intelligent Systems, 70569 Stuttgart, Germany; [b]Department of Mechanical Engineering, Carnegie Mellon University, Pittsburgh, PA 15213; [c]School of Mechanical and Aerospace Engineering, Nanyang Technological University, Singapore 639798, Singapore; and [d]School for Engineering of Matter, Transport and Energy, Arizona State University, Tempe, AZ 85287

Edited by John A. Rogers, University of Illinois, Urbana, IL, and approved August 8, 2016 (received for review May 22, 2016)

Shape-programmable matter is a class of active materials whose geometry can be controlled to potentially achieve mechanical functionalities beyond those of traditional machines. Among these materials, magnetically actuated matter is particularly promising for achieving complex time-varying shapes at small scale (overall dimensions smaller than 1 cm). However, previous work can only program these materials for limited applications, as they rely solely on human intuition to approximate the required magnetization profile and actuating magnetic fields for their materials. Here, we propose a universal programming methodology that can automatically generate the required magnetization profile and actuating fields for soft matter to achieve new time-varying shapes. The universality of the proposed method can therefore inspire a vast number of miniature soft devices that are critical in robotics, smart engineering surfaces and materials, and biomedical devices. Our proposed method includes theoretical formulations, computational strategies, and fabrication procedures for programming magnetic soft matter. The presented theory and computational method are universal for programming 2D or 3D time-varying shapes, whereas the fabrication technique is generic only for creating planar beams. Based on the proposed programming method, we created a jellyfish-like robot, a spermatozoid-like undulating swimmer, and an artificial cilium that could mimic the complex beating patterns of its biological counterpart.

programmable matter | multifunctional materials | soft robots | magnetic actuation | miniature devices

Shape-programmable matter refers to active materials that can be controlled by heat (1–5), light (6, 7), chemicals (8–13), pressure (14, 15), electric fields (16, 17), or magnetic fields (18–33) to generate desired folding or bending. As these materials can reshape their geometries to achieve desired time-varying shapes, they have the potential to create mechanical functionalities beyond those of traditional machines (1, 15). The functionalities of shape-programmable materials are especially appealing for miniature devices whose overall dimensions are smaller than 1 cm as these materials could significantly augment their locomotion and manipulation capabilities. The development of highly functional miniature devices is enticing because, despite having only simple rigid-body motions (34–36) and gripping capabilities (37), existing miniature devices have already been used across a wide range of applications pertaining to microfluidics (38, 39), microfactories (40, 41), bioengineering (42, 43), and health care (35, 44).

Among shape-programmable matter, the magnetically actuated materials are particularly promising for creating complex time-varying shapes at small scales because their control inputs, in the form of magnetic fields, can be specified not only in magnitude but also in their direction and spatial gradients. Furthermore, as they can be fabricated with a continuum magnetization profile, **m**, along their bodies, these magnetic materials can also generate deformations with very high spatial resolutions. A continuum **m** can be approximated as a collection of magnetic dipoles continuously distributed within a material, where each dipole can produce locally varying stress when it interacts with the actuating fields. The actuating fields can deform the materials by either exerting magnetic forces (27, 30) or torques (18, 19) on these dipoles.

Although shape-programmable magnetic soft materials have great potential, previous work can only rely on human intuition to approximate the required **m** and actuating fields for these materials to achieve their desired time-varying shapes. As a result, such heuristic and unsystematic methods can only program these materials for a limited number of applications, demonstrating only either simple deformations (21, 24–28) or very specific functionalities (18–20, 22, 23, 29–33).

Here, we present a universal programming methodology that can automatically generate the required **m** and actuating fields for small-scale soft matter to achieve desired time-varying shapes (Fig. 1*A*). This universal method therefore has the potential to inspire a wide variety of miniature devices that could transform robotics, material science, and biomedicine. The proposed method consists of theoretical formulations, computational strategies, and fabrication procedures. Although the theory and computational method are universal for programming 2D or 3D time-varying shapes (*S2. Programming Materials with 3D Time-Varying Shapes*), our fabrication technique is only generic for making planar beams. Despite the limitations of our current fabrication technique, it is still significantly better than existing techniques, which at most can only create direction-varying **m** that have a uniform magnitude (18, 19). As we can fabricate continua **m** that have desirable nonuniform magnitude and orientation profiles, the potential of shape-programmable magnetic beams can now be fully realized.

Programming Methodology

We demonstrate our programming methodology with a large deflecting beam subjected to quasistatic conditions (Fig. 1*B*). For practical considerations, we have also considered **m** to be time invariant and actuating fields to be uniform in space. These constraints are necessary because it is challenging both to remagnetize

Significance

At small scales, shape-programmable magnetic materials have significant potential to achieve mechanical functionalities that are unattainable by traditional miniature machines. Unfortunately, these materials have only been programmed for a small number of specific applications, as previous work can only rely on human intuition to approximate the required magnetization profile and actuating magnetic fields for such materials. Here, we propose a universal programming methodology that can automatically generate the desired magnetization profile and actuating fields for soft materials to achieve new time-varying shapes. The proposed method can enable other researchers to fully capitalize the potential of shape-programming technologies, allowing them to create a wide range of novel soft active surfaces and devices that are critical in robotics, material science, and medicine.

Author contributions: G.Z.L., Z.Y., X.D., H.M., and M.S. designed research; G.Z.L., Z.Y., X.D., H.M., O.E., and W.H. performed research; G.Z.L., Z.Y., and X.D. analyzed data; G.Z.L. and Z.Y. developed the theory; G.Z.L. and X.D. implemented the computational approach; and G.Z.L., Z.Y., X.D., H.M., W.H., and M.S. wrote the paper.

Conflict of interest statement: A European patent application related to this article has been recently filed by the Max Planck Institute for Intelligent Systems.

This article is a PNAS Direct Submission.

Freely available online through the PNAS open access option.

[1]G.Z.L., Z.Y., and X.D. contributed equally to this work.

[2]To whom correspondence should be addressed. Email: sitti@is.mpg.de.

This article contains supporting information online at www.pnas.org/lookup/suppl/doi:10.1073/pnas.1608193113/-/DCSupplemental.

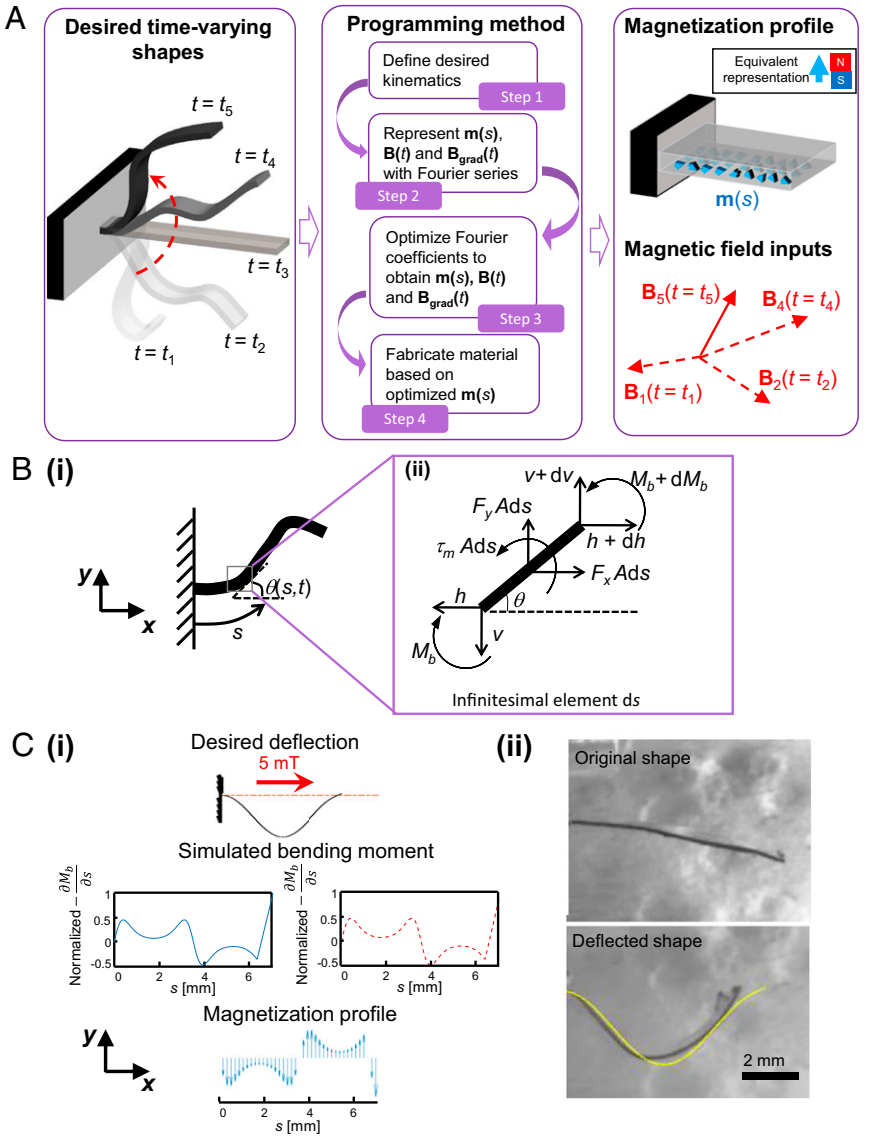

Fig. 1. The programming methodology and a simple proof of concept. (*A*) The programming method for magnetic soft elastomeric composite materials to achieve the desired time-varying shapes. We illustrate this concept with an arbitrary beam that can be programmed to achieve the desired shapes shown on the *Left*. By using our proposed programming method (shown in the *Center*), we can automatically generate the required magnetization profile, $\mathbf{m}(s)$, and magnetic field control inputs, $\mathbf{B}(t)$, for the material (shown on the *Right*). The given $\mathbf{m}(s)$ and $\mathbf{B}(t)$ are only used as an illustration. (*B*) A graphical illustration for the theoretical formulations. Based on the desired kinematics in *i*, a quasistatic analysis can be conducted on *ii*. (*C*) A simple proof of concept of the proposed method in which a beam is programmed to create a shape resembling a cosine function when it is subjected to a 5-mT uniform magnetic field input. (*i*) Desired shape, simulated first derivative of the bending moment, and necessary magnetization profile along the beam. The desired first derivative of the bending moment is represented by the blue curve, whereas the dotted red curve represents the first derivative of the bending moment generated by magnetic actuation. As the blue and dotted red curves will totally overlap one another, they have been separated into two plots for clarity. The plotted magnetization profile is along the predeformed beam (see Fig. S6 for a more quantitative representation for the magnetization). Additional parameters for this device can be found in *S9. Parameters for Each Case* and Table S1. The obtained experimental results are shown in *ii*. The yellow line represents the desired programmed shape for this demonstration. The beam achieved its programmed shape when it was subjected to a 5-mT magnetic field.

the device in situ and to create position-variant actuating fields at such small scale with our electromagnets (Fig. S1).

To simplify our discussion, we constrain the cross-sectional area of this beam to be uniform and allow it to bend in a plane. Furthermore, although we have provided the generic discussions for the beam's boundary conditions in *S1. Boundary Conditions* (see also Fig. S2), here we simplify the boundary conditions to fixed-free (Fig. 1*Bi*). Without any loss in generality, the bending axis of the beam is described by the z axis of the global frame shown in Fig. 1*B*.

Theoretical Formulation. Following the steps in Fig. 1*A*, we first define the desired deformations along the beam's length, s. Because such deformations can vary with time, t, the kinematics can be mathematically represented with the rotational deflections along the beam, $\theta(s,t)$ (Fig. 1*Bi*). After the kinematics are specified, we establish the torque balance equation for an arbitrary infinitesimal element (Fig. 1 *B, ii*), ds, at any time, t, to be as follows:

$$\tau_m A + v\cos\theta - h\sin\theta = -\frac{\partial M_b}{\partial s}. \quad [1]$$

The variables $\tau_m(s,t)$, $M_b(s,t)$, and A represent the applied magnetic torque (per volume), the beam's bending moment, and its cross-sectional area, respectively. The other variables,

$h(s,t)$ and $v(s,t)$, correspond to the x- and y-axis internal forces within the beam, respectively. Similarly, the force balance equations of the infinitesimal element can be expressed as follows:

$$F_x = -\frac{1}{A}\frac{\partial h}{\partial s}, \quad F_y = -\frac{1}{A}\frac{\partial v}{\partial s}, \tag{2}$$

where $F_x(s,t)$ and $F_y(s,t)$ represent the applied magnetic forces (per volume) along the x and y axes, respectively. Thus, by using the Euler–Bernoulli equation and substituting Eq. **2** into Eq. **1**, the desired deflections (i.e., required first derivative of bending moment) can be expressed explicitly by the actuating magnetic forces and torques as follows:

$$\tau_m + \int_s^L F_y \, ds \cos\theta - \int_s^L F_x \, ds \sin\theta = -\frac{EI}{A}\frac{\partial^2\theta}{\partial s^2}. \tag{3}$$

The variables E, I, and L represent the Young's modulus, the second moment of area, and the length of the beam, respectively. Eq. **3** implies that the material's desired time-varying shapes can be achieved if the magnetic torques and forces can be programmed to balance the desired first derivative of bending moment, across the entire length of the beam at all times. To determine the necessary $\mathbf{m}(s)$ and actuating fields for the desired $\theta(s,t)$, we first give their mathematical relationship with the applied magnetic torques and forces:

$$\begin{aligned} \tau_m(s,t) &= [0 \quad 0 \quad 1]\{[\mathbf{R}(s,t)\mathbf{m}(s)] \times \mathbf{B}(t)\}, \\ F_x(s,t) &= [1 \quad 0 \quad 0]\{[\mathbf{R}(s,t)\mathbf{m}(s)] \cdot \nabla\}\mathbf{B}(t), \\ F_y(s,t) &= [0 \quad 1 \quad 0]\{[\mathbf{R}(s,t)\mathbf{m}(s)] \cdot \nabla\}\mathbf{B}(t). \end{aligned} \tag{4}$$

The magnetic torque is a function of $\mathbf{m}(s)$ and the magnetic field, $\mathbf{B}(t)$, whereas the magnetic forces are dependent on $\mathbf{m}(s)$ and the spatial gradients of $\mathbf{B}(t)$. The rotational matrix, $\mathbf{R}(s,t)$, is used to account for the orientation change of magnetization profile due to the beam's large deflection, and it is given as the following:

$$\mathbf{R} = \begin{bmatrix} \cos\theta & -\sin\theta & 0 \\ \sin\theta & \cos\theta & 0 \\ 0 & 0 & 1 \end{bmatrix}. \tag{5}$$

Computational Method. In contrast to previous magnetic programming studies, we do not use human intuition to speculate the necessary $\mathbf{m}(s)$ and the actuating fields. Instead, they are automatically generated by computers, and this is achieved by first representing them with corresponding sets of 1D Fourier series (step 2 in Fig. 1*A*):

$$\begin{aligned} \mathbf{m}(s) &= \begin{bmatrix} \sum_{i=0}^{n} a_i \cos(iw_s s) + b_i \sin(iw_s s) \\ \sum_{i=0}^{n} c_i \cos(iw_s s) + d_i \sin(iw_s s) \\ 0 \end{bmatrix}, \\ \mathbf{B}(t) &= \begin{bmatrix} \sum_{j=0}^{m} \alpha_j \cos(jw_t t) + \beta_j \sin(jw_t t) \\ \sum_{j=0}^{m} \gamma_j \cos(jw_t t) + \eta_j \sin(jw_t t) \\ 0 \end{bmatrix}, \\ \mathbf{B}_{\text{grad}}(t) &= \begin{bmatrix} \frac{\partial B_x}{\partial x}(t) \\ \frac{\partial B_y}{\partial x}(t) \\ \frac{\partial B_y}{\partial y}(t) \end{bmatrix} = \begin{bmatrix} \sum_{j=0}^{m} \epsilon_j \cos(jw_t t) + \delta_j \sin(jw_t t) \\ \sum_{j=0}^{m} \lambda_j \cos(jw_t t) + \mu_j \sin(jw_t t) \\ \sum_{j=0}^{m} \rho_j \cos(jw_t t) + \sigma_j \sin(jw_t t) \end{bmatrix}. \end{aligned} \tag{6}$$

The significant benefit of such representation is that Fourier series is inclusive of all possible discrete or continuous mathematical functions, enabling our proposed method to be universal. The vector $\mathbf{B}_{\text{grad}}(t)$ represents the spatial gradients of $\mathbf{B}(t)$ necessary for generating F_x and F_y. The angular frequencies, ω_s and ω_t, are given as $2\pi/L$ and $2\pi/T$, respectively, and T represents the total time to complete the shape trajectory. The other variables $a_i, b_i, c_i, d_i, \alpha_j, \beta_j, \gamma_j, \eta_j, \epsilon_j, \delta_j, \lambda_j, \mu_j, \rho_j,$ and σ_j are the 1D Fourier coefficients, and their subscripts i and j are integers that range from 0 to n and 0 to m, respectively. Thus, by substituting Eq. **6** and Eq. **4** into Eq. **3**, we can obtain the following equation:

$$\begin{aligned} &[\mathcal{F}_1 \cos\theta - \mathcal{F}_2 \sin\theta] + \left[\int_s^L \mathcal{F}_3 \cos\theta + \mathcal{F}_4 \sin\theta \, ds\right]\cos\theta \\ &\quad - \left[\int_s^L \mathcal{F}_5 \cos\theta + \mathcal{F}_6 \sin\theta \, ds\right]\sin\theta = -\frac{EI}{A}\frac{\partial^2\theta}{\partial s^2}, \end{aligned} \tag{7}$$

where the left side is a function that represents the magnetic actuation and the right side represents the desired first derivative of bending moment. Each of these symbols, $\mathcal{F}_1$ to $\mathcal{F}_6$, corresponds to a set of 2D Fourier series expressed in s and t, with each 2D Fourier coefficients created from the 1D Fourier coefficients in $\mathbf{m}(s)$, $\mathbf{B}(t)$, and $\mathbf{B}_{\text{grad}}(t)$. Although the detailed mathematical description for $\mathcal{F}_2$ to $\mathcal{F}_6$ are shown in *S6. Additional Discussion*, we will show the mathematical representation of $\mathcal{F}_1$ here as an example:

$$\begin{aligned} \mathcal{F}_1 = &\sum_{i=0}^{n}\sum_{j=0}^{m}\left(a_i\gamma_j - c_i\alpha_j\right)\cos(i\omega_s s)\cos(j\omega_t t) \\ &+ \sum_{i=0}^{n}\sum_{j=0}^{m}\left(a_i\eta_j - c_i\beta_j\right)\cos(i\omega_s s)\sin(j\omega_t t) \\ &+ \sum_{i=0}^{n}\sum_{j=0}^{m}\left(b_i\gamma_j - d_i\alpha_j\right)\sin(i\omega_s s)\cos(j\omega_t t) \\ &+ \sum_{i=0}^{n}\sum_{j=0}^{m}\left(b_i\eta_j - d_i\beta_j\right)\sin(i\omega_s s)\sin(j\omega_t t). \end{aligned} \tag{8}$$

By following step 3 in Fig. 1*A*, a computational optimization method is then used to determine the optimal values of the 1D Fourier coefficients to satisfy Eq. **7**. This optimization method is implemented by first discretizing the motion of the beam into p time frames, that is, $t = t_1; \ldots; t = t_p = T$. Meanwhile, the beam is divided into q segments in length, that is, $s = s_1; \ldots; s = s_q = L$. Thus, we create q new equations for each time frame by substituting different values of s along the beam into Eq. **7**. By assembling all of the equations across all time frames, there are a total of $p \times q$ linear equations that can be written in matrix form as follows:

$$\mathbf{Ku} = \mathbf{M_b}, \tag{9}$$

where $\mathbf{u}$ and $\mathbf{M_b}$ are vectors containing the 2D Fourier coefficients and the desired first derivative of the bending moment across these $p \times q$ equations, respectively.

Subsequently, the optimal 1D Fourier coefficients in $\mathbf{m}(s)$, $\mathbf{B}(t)$, and $\mathbf{B}_{\text{grad}}(t)$ can be solved by performing the following optimization process:

$$\begin{aligned} \text{minimize} \quad & (\mathbf{Ku} - \mathbf{M_b})^{\mathrm{T}}\mathbf{Q}(\mathbf{Ku} - \mathbf{M_b}) \\ \text{subjected to:} \quad & |\mathbf{m}(s)| \le m_{\max}, \\ & |\mathbf{B}(t)| \le B_{\max}, \\ & |\mathbf{B}_{\text{grad}}(t)| \le B_{\text{grad max}}, \end{aligned} \tag{10}$$

where $\mathbf{Q}$ is a matrix that gives higher weightings to time frames that are deemed to be more important. Physically, the optimization

process in Eq. **10** minimizes the difference between the magnetic actuation and the desired first derivative of the bending moment while subjected to the physical constraints of our systems. After this optimization process has been solved numerically by solvers such as genetic algorithm (45) and gradient-based solvers (46), the optimal $\mathbf{m}(s)$, $\mathbf{B}(t)$, and $\mathbf{B}_{\text{grad}}(t)$ will be obtained.

Fabrication Technique. Based on the magnitude profile of $\mathbf{m}(s)$ determined above, we use a two-step molding process to embed a heterogeneous distribution of ferromagnetic and aluminum microparticles into a silicone rubber. A large magnitude of magnetization is created by locally increasing the concentration of ferromagnetic particles, whereas a desired orientation profile for $\mathbf{m}(s)$ can be created by magnetizing the material when it is sandwiched between two jigs of a specified curvature. This curvature can be represented by the following integral:

$$x_{\text{jig}}(s) = \int_0^s \cos(\phi(s))\mathrm{d}s,$$
$$y_{\text{jig}}(s) = \int_0^s \sin(-\phi(s))\mathrm{d}s, \qquad [11]$$

where $\phi(s) = \tan^{-1}((m_y(s))/(m_x(s)))$, and m_x and m_y are the x- and y-axis components of $\mathbf{m}(s)$ when the material is undeformed. After magnetizing the material, its desired $\mathbf{m}(s)$ can be obtained (step 4 in Fig. 1*A*; see *Materials and Methods* for more details).

Results

For the first experimental demonstration of our shape-programming methodology, a millimeter-scale beam was programmed to create a shape that resembled a cosine function when it was actuated by a constant magnetic field (Fig. 1 *C i* and *ii*). Next, we programmed a beam to produce a simple sequence of time-varying shapes with 100 discrete time frames. In each time frame, a uniform curvature was held over the beam, gradually increasing between each frame, until the beam curled into a semicircle (Fig. 2*A*). Despite the large number of time-varying shapes, we obtained a simple $\mathbf{m}(s)$ as well as actuating fields that satisfied Eq. **7** (Fig. 2 *B* and *C*). The beam was then fabricated and experimentally manipulated to achieve its desired shapes (Fig. 2*D*). Because the required magnetization profile and actuating fields were relatively simple, we extended this concept to simultaneously control multiple beams that have similar motions. By properly configuring several such beams, we were able to reversibly bend them into a "CMU" logo shape (Fig. 2*E* and Movie S1). We further extended this concept by using two similar beams to form the tentacles of a jellyfish-like robot. These tentacles could generate a fast power stroke and a slow recovery stroke for the robot to swim against the slope of an oil–water interface (average speed, 1.8 mm/s; see also Fig. 2*F*, Movie S2, and *S6. Additional Discussion*, for controlling the stroke speeds). The jellyfish-like robot was also steerable, and these steering strategies are discussed in *S3. Steering Strategies* and Fig. S3.

We had also programmed a spermatozoid-like undulating swimmer. To make this swimming gait more biomimetic than previous spermatozoid-like robots (22), we specified the gait to be a propagating traveling wave, with an amplitude that increases linearly from the fixed end to the free end (Fig. 3*A*). Despite the complexity of the gait, our programming method could obtain the necessary $\mathbf{m}(s)$ and actuating fields for the undulating swimmer (Fig. 3 *B* and *C*). After fabricating this swimmer, we experimentally show that it could use this gait to swim on an air–water interface (average speed, 11 mm/s; Fig. 3*D* and Movie S3).

Finally, we created an artificial soft cilium that was able to approximate the complex beating pattern of a biological cilium (47). This beating pattern was divided into two strokes—the power and the recovery strokes (Fig. 4*A*). Due to the complexity of this motion, the optimization problem for obtaining $\mathbf{m}(s)$ and the actuating fields became highly nonconvex, containing many suboptimal solutions. The solution would be easily trapped and difficult to jump out from a suboptimal solution if we used only one optimization process to solve for the large number of design variables simultaneously (46). Hence, we used a multistep optimization approach that is similar to the previously reported ones in refs. 48 and 49 to divide the original optimization problem into two sequential optimization processes, allowing each process to solve for one subset of the design variables. As there are more design variables in the first optimization process than the second one (Fig. S4), we would have higher chances of obtaining a more accurate result for the more complicated optimization process if we solve it first. Therefore, our first optimization process was to determine the necessary $\mathbf{m}(s)$ and actuating fields for the more complex recovery stroke. The obtained $\mathbf{m}(s)$ was subsequently fed into a second optimization process that determined the required actuating fields for the simpler power stroke. Here, the power stroke was simpler than the recovery stroke because its desired first derivative of bending moment has fewer changes across the time frames, making it easier to use Eq. **7** to program them. The obtained results for the artificial cilium are shown in Fig. 4 *B–D* and Movie S4, and the key time-varying shapes that we used to closely mimic the complex beating pattern of a biological cilium were shown in Fig. 4*A*. Although other researchers have had some success in creating time-asymmetrical motions for their artificial cilia (50–53), our artificial cilium is the only one on a millimeter scale that can approximate the motions of a biological cilium.

Discussion

Although the proposed programming methodology is promising, there are several limitations that need to be addressed in future studies. First, our method cannot produce all possible time-varying shapes when $\mathbf{m}(s)$ is time invariant and the actuating fields are position invariant as each of them can only be specified with a 1D Fourier series. This phenomenon can be explained from the magnetic actuation function in Eq. **7**, which can be mathematically described as a function of six sets of 2D Fourier series. As all of the 2D Fourier coefficients in this function are created from the lower-dimensional 1D Fourier coefficients of $\mathbf{m}(s)$ and the actuating magnetic fields, many of these 2D Fourier coefficients become coupled with one another and cannot be arbitrarily specified. Thus, despite encompassing six sets of 2D Fourier series, the generated magnetic actuation can only represent a subset of 2D functions that are expressed in terms of s and t. This means that we can only program time-varying shapes whose first derivative of bending moment can be expressed in 2D functions, which are representable by the magnetic actuation function. Although a complete analysis to quantify the range of time-varying shapes achievable by our method is beyond the scope of this paper, we have provided a brief discussion on this topic in *S4. Achievable Time-Varying Shapes*. To better understand the range of achievable time-varying shapes, we will formulate a mathematical model to quantify this range in the future. As another future work, we will also increase the range of achievable shapes by developing more powerful electromagnets that can enable the actuating fields to become position variant (*S6. Additional Discussion*).

Second, because several metastable shapes may exist for a given control input, the programmable material may deform into an undesired shape. However, because the selected metastable shape is highly dependent on the previous shape, this limitation can be moderated by using a finer temporal resolution for the shape trajectories. This moderation reduces the deviation between

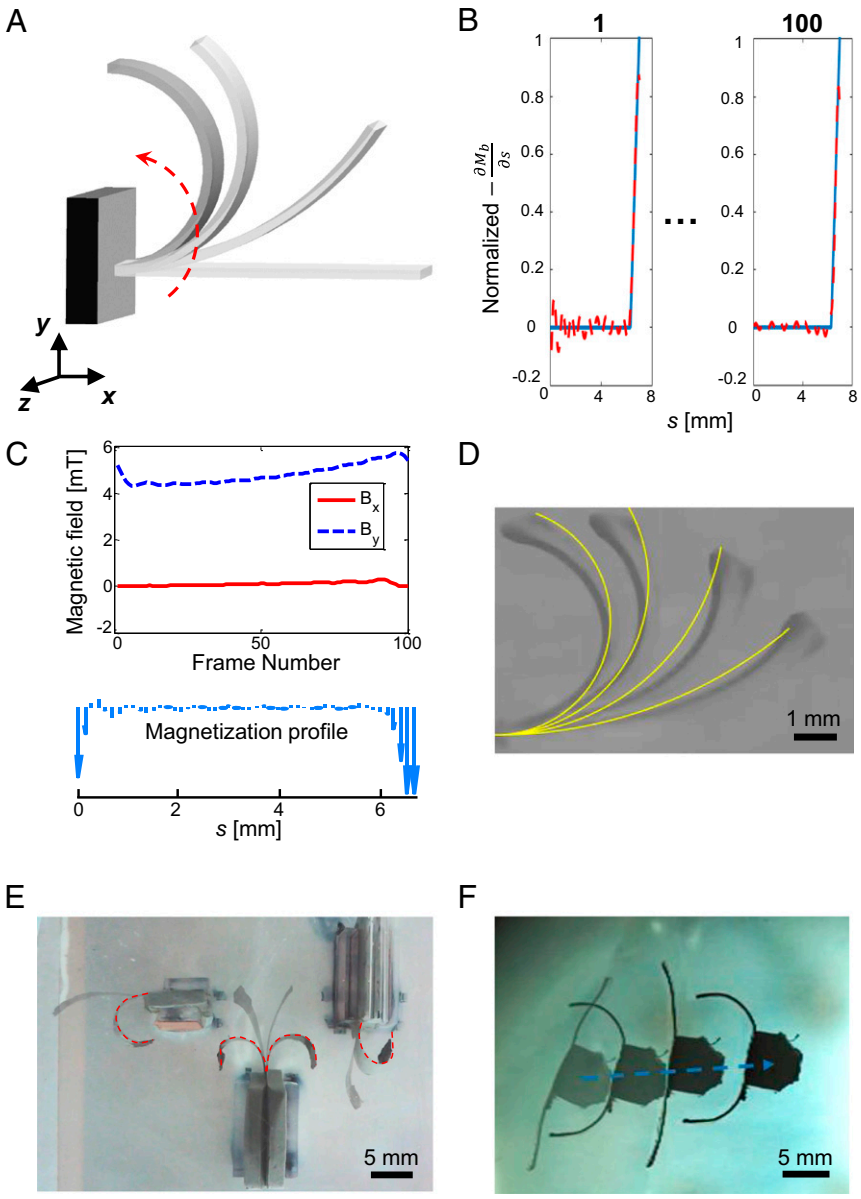

Fig. 2. Programming soft composite materials that can gradually fold up into a semicircle. (*A*) Schematic of a soft beam programmed to fold up under magnetic excitation. Although we illustrated this motion with only four shapes, there were a total of 100 distinct shapes throughout this motion. (*B*) Optimization results for the desired first derivative of the bending moment. Each plot represents the desired first derivative of the bending moment of the beam for one time frame. The frame number for each time frame is represented by the number at the *Top*. In the simulations, the time difference between each time frame is 0.01 s. The blue lines in the time frames represent the desired first derivative of the bending moment, and the dotted red lines represent the obtained first derivative of the bending moment created by the magnetic actuation. The *x* axis of each plot represents the length of the beam, which ranges from $s = 0$ to 7 mm. (*C*) The required magnetization profile, $\mathbf{m}(s)$, and the magnetic field, $\mathbf{B}(t)$, to achieve the desired time-varying shapes. This magnetization profile is along the predeformed straight beam (see Fig. S6 for a more quantitative representation for the magnetization profile). Using the coordinate system in *A* as a reference, the variables B_x and B_y in the magnetic field plot represent the *x*- and *y*-axis components of the magnetic field, respectively. (*D*) Snapshots of a single beam curling up under magnetic excitation. The yellow lines represent the corresponding desired time-varying shapes. (*E*) Four soft beams made of the programmable material are shown deforming into a reversible CMU logo under magnetic excitation. To visualize the logo better, we highlighted the final CMU shape with dotted red lines. (*F*) A jellyfish-like robot equipped with two soft tentacles made of the programmable soft composite material. The robot could propel itself on an oil–water interface by bending its tentacles back and forth under magnetic excitation. Additional parameters for this device can be found in *S9. Parameters for Each Case* and Table S1.

the desired shape and the previous shape, making it easier to guide the material to deform into the desired shape.

Third, due to finite computational power, it is still an open challenge to obtain a global solution from highly nonconvex optimization problems, which have many design variables (46). As a result, we can only rely on numerical techniques such as the two-step optimization approach to moderate this challenge. Although this approach may allow us to obtain more accurate suboptimal solutions, it may also overconstrain the optimization problem unnecessarily and cause a reduction in the original search space (*S5. Discussion for Two-Step Optimization Approach* and Fig. S4). Therefore, we should only implement the two-step optimization approach when we cannot obtain an accurate solution with one optimization process. In view of this challenge, in the

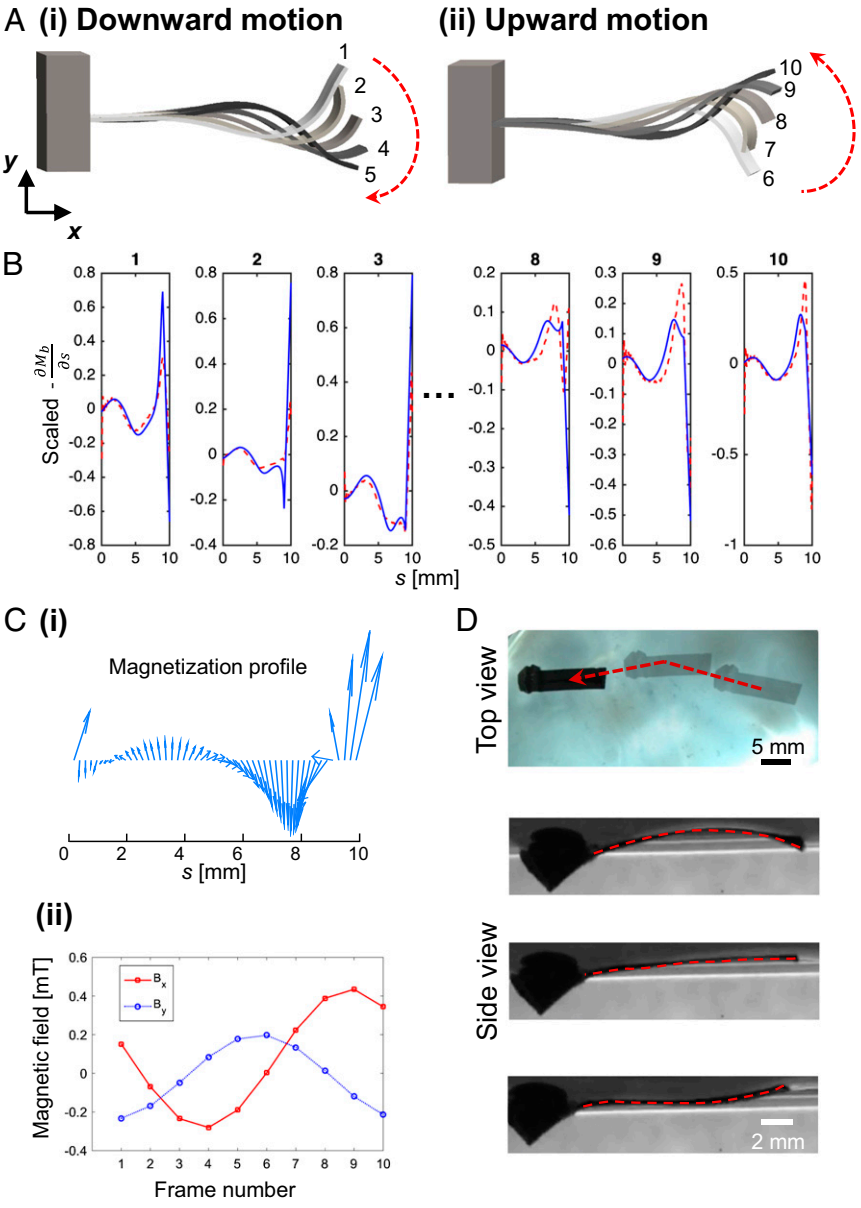

Fig. 3. Programming a spermatozoid-like undulating soft swimmer. (*A*) The desired undulation, which requires a traveling wave with increasing amplitude from the left tip to the right tip. The entire motion can be divided into two strokes: (*i*) downward motion and (*ii*) upward motion. The associated time frame for each shape is represented by a corresponding frame number. In the simulations, the time difference between each time frame is 0.1 s. (*B*) Optimization results for the desired first derivative of the bending moment to achieve the undulation. Each plot represents the desired first derivative of the bending moment of the beam for one time frame. The frame number is represented by the number at the top. The blue lines represent the desired first derivative of the bending moment, and the dotted red lines represent the obtained first derivative of the bending moment created by the magnetic actuation. The *x* axis for each frame corresponds to the length of the beam, which ranges from $s = 0$ to 10 mm. (*C*) The required (*i*) magnetization profile and (*ii*) magnetic field for the swimmer. This is the magnetization profile along the predeformed beam (see Fig. S6 for a more quantitative representation for the magnetization profile). Using the coordinate system in *A* as a reference, the variables B_x and B_y in the magnetic field plot represent the *x*-axis and *y*-axis components of the magnetic field, respectively. (*D*) Snapshots extracted from the movie of the undulating swimmer swimming on an air–water interface—top view and side view of the swimmer. Additional parameters for this device can be found in *S9. Parameters for Each Case* and Table S1.

future we will also investigate new numerical techniques, allowing us to obtain more accurate solutions for a highly nonconvex optimization problem.

Fourth, our fabrication technique, the two-step molding process shown in Fig. 5 *A–D*, is only capable of tuning the amount of magnetic particles along the in-plane axis of the beams. Because we cannot tune the amount of magnetic particles along all axes of a structure, we are still unable to create an **m** that has a desirable nonuniform magnitude profile in 3D, preventing us from fabricating structures that can achieve specific 3D time-varying shapes. Furthermore, we could not program beams smaller than the millimeter-scale because it becomes difficult to manually sandwich such small-scale beams into the jigs during the magnetization process (Fig. 5*F*). We will explore new microfabrication processes that will allow us to create smaller-scale structures with desirable **m** that have 3D nonuniform magnitude profile.

Fifth, although our proposed computational method is not restricted to creating miniature devices, we have yet to use it for macroscale devices. Nevertheless, the procedures for constructing

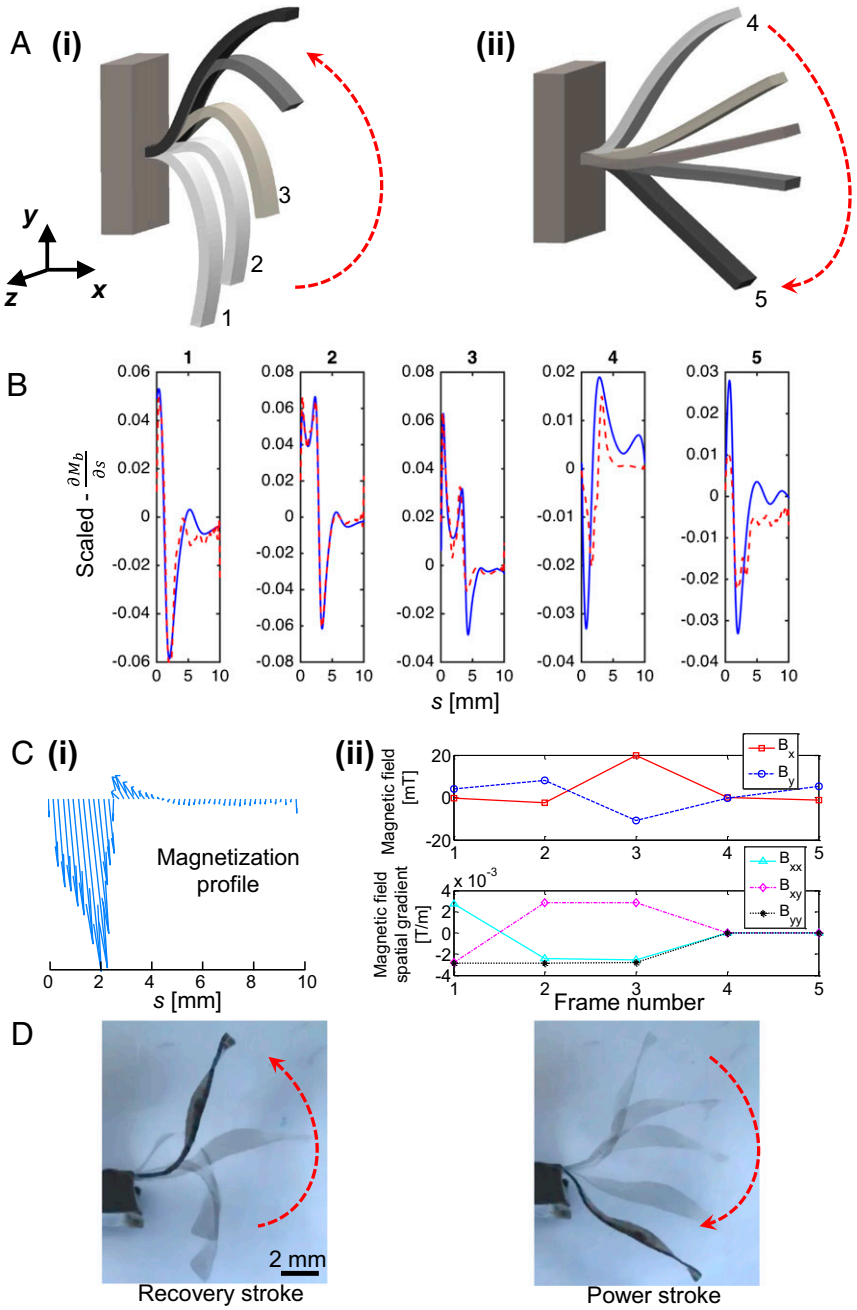

Fig. 4. Programming an artificial cilium. (*A*) Extracted 2D natural cilia motion as expressed in Cartesian coordinates. The motion pattern includes two strokes: (*i*) the recovery stroke and (*ii*) the power stroke. The key time frames used by the artificial cilium are associated with a corresponding frame number. The time difference between each time frame is 0.2 s. (*B*) Optimization results for the desired first derivative of the bending moment to achieve the cilium motion. Each plot represents the desired first derivative of the bending moment of the beam for one time frame. The frame number is represented by the number at the top of it. The blue lines represent the desired first derivative of the bending moment, and the dotted red lines represent the obtained first derivative of the bending moment created by the magnetic actuation. The *x* axis for each frame corresponds to the length of the beam, ranging from $s = 0$ to 10 mm. The first three frames were given more weight during the optimization process because they were deemed to be more important. (*C*, *i*) The required magnetization profile and (*ii*) the magnetic field and its spatial gradients for the cilium (see Fig. S6 for a more quantitative representation for the magnetization profile). Using the coordinate system in *A* as a reference, the variables B_x and B_y in the magnetic field plot represent the *x*-axis and *y*-axis components of the magnetic field, respectively. The spatial gradients B_{xx}, B_{xy}, and B_{yy} represent $\partial B_x/\partial x$, $\partial B_x/\partial y$, and $\partial B_y/\partial y$, respectively. (*D*) Snapshots extracted from the movie of the beating artificial cilium. Additional parameters for this device can be found in *S9. Parameters for Each Case* and Table S1.

such macroscale devices are discussed in *S6. Additional Discussion*, and the implementation for these procedures will be explored as a future work.

In summary, we have introduced a universal programming methodology that can enable scientists and engineers to magnetically program desired time-varying shapes for soft materials. The method was validated with a simple showcase, and we demonstrated its versatility by creating a reversible CMU logo, a jellyfish-like robot, a spermatozoid-like undulating swimmer, and an artificial cilium. Compared with other shape-programmable materials that may require minutes to induce a shape change (4, 8), our devices can transform into their desired shapes within

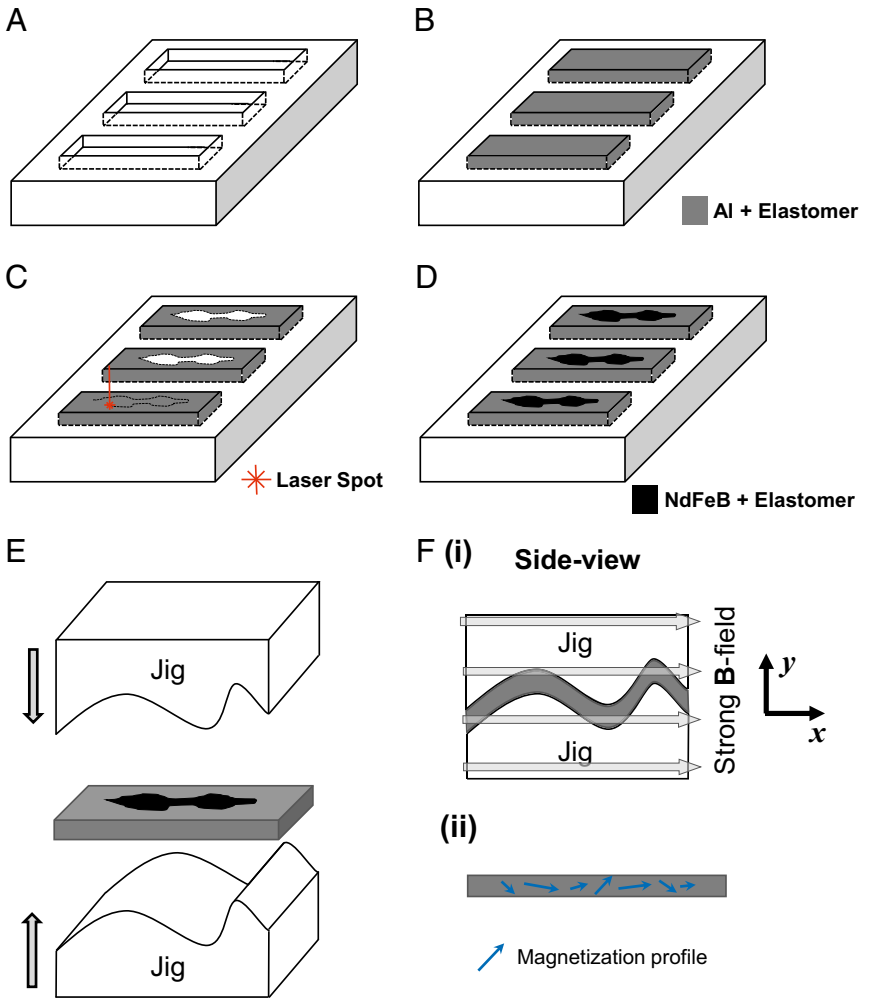

Fig. 5. The fabrication procedure to create a programmable magnetic soft composite beam: (*A*) a negative mold for the beam; (*B*) the passive component, Al plus Ecoflex, was poured into the mold in liquid form and allowed to cure; (*C*) based on the magnitude profile of $\mathbf{m}(s)$, a band of nonuniform width was cut out with a laser cutter; (*D*) the active component, NdFeB plus Ecoflex, was then poured and cured to replace the band; (*E*) the beam was bent into the jig profile; (*F*, *i*) the beam was magnetized with a strong B field ($\sim$ 1 T); (*ii*) the desired $\mathbf{m}(s)$ will be created after the beam was removed from the jig.

seconds. We envision that this methodology may enable researchers to develop a wide range of novel soft programmable active surfaces and devices that can find broad applications in robotics, engineering, and biomedicine.

Materials and Methods

Here, we provide a detailed discussion for our fabrication technique. The required steps to create the desired magnetization profile for a programmable beam are summarized in Fig. 5. The programmable magnetic soft composite material consists of two components: a passive component and an active component that can be stimulated by magnetic excitation. The active component is created by embedding fine neodymium–iron–boron (NdFeB) particles that have an average size of 5 μm (MQFP; Magnequench) into a soft silicone rubber (Ecoflex 00-10; Smooth-on, Inc.). The volume ratio for the NdFeB particles and Ecoflex 00-10 is 0.15:1. The passive component is created by embedding aluminum (Al) powder with an average particle size of 5 μm into the same type of silicone rubber with the same volume ratio. The volume ratio is selected to ensure that the elastic modulus of the active and passive components are identical, allowing the composite to have a uniform elastic modulus. The relationship between the passive component's volume ratio and its resultant elastic modulus was experimentally characterized (*S7. Matching the Elastic Modulus Properties* and Fig. S5).

To create a nonuniform $\mathbf{m}(s)$ that has a desired magnitude profile, the distribution between the passive and active components must be patterned. The locations that have a higher magnitude of magnetization will have more active components. To achieve this, a two-step micromolding process is adopted. First, a negative mold with the desired beam geometries is created by computer numerical control machining on an acrylic sheet (Fig. 5*A*). The passive component (in liquid form) is poured into the negative mold and is allowed to cure (Fig. 5*B*). Once the passive component is fully cured, a laser cutter is used to cut out a band with nonuniform width (Fig. 5*C*). The active component (in liquid form) is poured into the mold to replace the removed band (Fig. 5*D*). The two components form a composite of a uniform thickness once the active component is cured. Due to the nonuniform width of the band, the distribution of the active components can be patterned. This allows the beam to have an $\mathbf{m}(s)$ with a desired magnitude profile after the beam is magnetized. The desired orientation profile of $\mathbf{m}(s)$ is created by using laser-cut jigs to bend/fold the beam during the magnetization process (Fig. 5 *E* and *Fi*). Thus, by magnetizing the beam when it is sandwiched between the jigs, the desired orientation profile can be obtained after the applied magnetizing field and the jigs are removed (Fig. 5 *F*, *ii*). The NdFeB particles that are embedded within the active components will be saturated by the large uniform magnetizing field ($\sim$ 1 T), creating the desired $\mathbf{m}(s)$ for the material.

ACKNOWLEDGMENTS. We acknowledge Carmel Majidi for modeling discussions and Burak Ozdoganlar and Emrullah Korkmaz for their help with fabricating the precision molds for our soft devices. Furthermore, we thank Steven Rich, Zeinab Hosseini-Doust, and Lindsey Hines for their useful suggestions on the paper's language. We also thank members of the Nano-Robotics Laboratory at Carnegie Mellon University and the Physical Intelligence Department at the Max Planck Institute for Intelligent Systems for their helpful discussions. This work was partially supported by National Science Foundation National Robotics Initiative Program Grant 1317477.

1. Felton S, Tolley M, Demaine E, Rus D, Wood R (2014) Applied origami. A method for building self-folding machines. *Science* 345(6197):644–646.
2. Hawkes E, et al. (2010) Programmable matter by folding. *Proc Natl Acad Sci USA* 107(28):12441–12445.
3. Mohr R, et al. (2006) Initiation of shape-memory effect by inductive heating of magnetic nanoparticles in thermoplastic polymers. *Proc Natl Acad Sci USA* 103(10): 3540–3545.
4. Xie T (2010) Tunable polymer multi-shape memory effect. *Nature* 464(7286):267–270.
5. Huang HW, Sakar MS, Petruska AJ, Pané S, Nelson BJ (2016) Soft micromachines with programmable motility and morphology. *Nat Commun* 7:12263.
6. Liu Y, Boyles JK, Genzer J, Dickey MD (2012) Self-folding of polymer sheets using local light absorption. *Soft Matter* 8(6):1764–1769.
7. Mu J, et al. (2015) Origami-inspired active graphene-based paper for programmable instant self-folding walking devices. *Sci Adv* 1(10):e1500533.
8. Erb RM, Sander JS, Grisch R, Studart AR (2013) Self-shaping composites with programmable bioinspired microstructures. *Nat Commun* 4:1712.
9. Jeong K-U, et al. (2011) Three-dimensional actuators transformed from the programmed two-dimensional structures via bending, twisting and folding mechanisms. *J Mater Chem* 21(19):6824–6830.
10. Maeda S, Hara Y, Sakai T, Yoshida R, Hashimoto S (2007) Self-walking gel. *Adv Mater* 19(21):3480–3484.
11. Thérien-Aubin H, Moshe M, Sharon E, Kumacheva E (2015) Shape transformations of soft matter governed by bi-axial stresses. *Soft Matter* 11(23):4600–4605.
12. Wei Z, et al. (2014) Hybrid hydrogel sheets that undergo pre-programmed shape transformations. *Soft Matter* 10(41):8157–8162.
13. Ye C, et al. (2015) Self-(un) rolling biopolymer microstructures: Rings, tubules, and helical tubules from the same material. *Angew Chem Int Ed Engl* 54(29):8490–8493.
14. Martinez RV, Fish CR, Chen X, Whitesides GM (2012) Elastomeric origami: Programmable paper-elastomer composites as pneumatic actuators. *Adv Funct Mater* 22(7):1376–1384.
15. Rus D, Tolley MT (2015) Design, fabrication and control of soft robots. *Nature* 521(7553):467–475.
16. Hines L, Petersen K, Sitti M (2016) Inflated soft actuators with reversible stable deformations. *Adv Mater* 28(19):3690–3696.
17. Zhang C, Chen H, Liu L, Li D (2015) Modelling and characterization of inflated dielectric elastomer actuators with tubular configuration. *J Phys D Appl Phys* 48(24): 245502.
18. Diller E, Zhuang J, Lum GZ, Edwards MR, Sitti M (2014) Continuously distributed magnetization profile for millimeter-scale elastomeric undulatory swimming. *Appl Phys Lett* 104(17):174101.
19. Kim J, et al. (2011) Programming magnetic anisotropy in polymeric microactuators. *Nat Mater* 10(10):747–752.
20. Garstecki P, Tierno P, Weibel DB, Sagués F, Whitesides GM (2009) Propulsion of flexible polymer structures in a rotating magnetic field. *J Phys Condens Matter* 21(20): 204110.
21. Crivaro A, Sheridan R, Frecker M, Simpson TW, Von Lockette P (2016) Bistable compliant mechanism using magneto active elastomer actuation. *J Intell Mater Syst Struct* 27(15):2049–2061.
22. Dreyfus R, et al. (2005) Microscopic artificial swimmers. *Nature* 437(7060):862–865.
23. Jang B, et al. (2015) Undulatory locomotion of magnetic multilink nanoswimmers. *Nano Lett* 15(7):4829–4833.
24. Roche J, Von Lockette P, Lofland S (2011) Study of hard- and soft-magnetorheological elastomers (MRE's) actuation capabilities. *Proceedings of the 2011 COMSOL Conference in Boston* (COMSOL, Inc., Burlington, MA).
25. Khoo M, Liu C (2001) Micro magnetic silicone elastomer membrane actuator. *Sens Actuators A Phys* 89(3):259–266.
26. Olsson RT, et al. (2010) Making flexible magnetic aerogels and stiff magnetic nanopaper using cellulose nanofibrils as templates. *Nat Nanotechnol* 5(8):584–588.
27. Zrinyi M, Barsi L, Büki A (1997) Ferrogel: A new magneto-controlled elastic medium. *Polym Gels Netw* 5(5):415–427.
28. Zrınyi M, Szabó D, Kilian HG (1998) Kinetics of the shape change of magnetic field sensitive polymer gels. *Polym Gels Netw* 6(6):441–454.
29. Qiu T, et al. (2014) Swimming by reciprocal motion at low Reynolds number. *Nat Commun* 5:5119.
30. Fuhrer R, Schumacher CM, Zeltner M, Stark WJ (2013) Soft iron/silicon composite tubes for magnetic peristaltic pumping: Frequency-dependent pressure and volume flow. *Adv Funct Mater* 23(31):3845–3849.
31. Nguyen VQ, Ahmed AS, Ramanujan RV (2012) Morphing soft magnetic composites. *Adv Mater* 24(30):4041–4054.
32. Mitsumata T, Horikoshi Y, Negami K (2008) High-power actuators made of two-phase magnetic gels. *Jpn J Appl Phys* 47(9R):7257.
33. Zhang J, Diller E (2015) Millimeter-scale magnetic swimmers using elastomeric undulations. *2015 IEEE/RSJ International Conference on Intelligent Robots and Systems (IROS)* (IEEE, Hamburg, Germany), pp 1706–1711.
34. Diller E, Giltinan J, Lum GZ, Ye Z, Sitti M (2014) Six-Degrees-of-Freedom Remote Actuation of Magnetic Microrobots. *Proceedings of Robotics: Science and Systems* (Berkeley, CA). Available at www.roboticsproceedings.org/rss10/p13.html. Accessed July 16, 2014.
35. Kummer MP, et al. (2010) Octomag: An electromagnetic system for 5-dof wireless micromanipulation. *IEEE Trans Robot* 26(6):1006–1017.
36. Qiu F, et al. (2015) Magnetic helical microswimmers functionalized with lipoplexes for targeted gene delivery. *Adv Funct Mater* 25(11):1666–1671.
37. Diller E, Sitti M (2014) Three-dimensional programmable assembly by untethered magnetic robotic micro-grippers. *Adv Funct Mater* 24(28):4397–4404.
38. Ye Z, Diller E, Sitti M (2012) Micro-manipulation using rotational fluid flows induced by remote magnetic micro-manipulators. *J Appl Phys* 112(6):064912.
39. Khalil IS, Magdanz V, Sanchez S, Schmidt OG, Misra S (2014) The control of self-propelled microjets inside a microchannel with time-varying flow rates. *IEEE Trans Robot* 30(1):49–58.
40. Elbuken C, Khamesee MB, Yavuz M (2009) Design and implementation of a micromanipulation system using a magnetically levitated mems robot. *IEEE ASME Trans Mechatron* 14(4):434–445.
41. Khamesee MB, Kato N, Nomura Y, Nakamura T (2002) Design and control of a microrobotic system using magnetic levitation. *IEEE ASME Trans Mechatron* 7(1):1–14.
42. Sakar MS, et al. (2011) Modeling, control and experimental characterization of microbiorobots. *Int J Robot Res* 30(6):647–658.
43. Tasoglu S, Diller E, Guven S, Sitti M, Demirci U (2014) Untethered micro-robotic coding of three-dimensional material composition. *Nat Commun* 5:3124.
44. Sitti M (2009) Miniature devices: Voyage of the microrobots. *Nature* 458(7242): 1121–1122.
45. Booker LB, Goldberg DE, Holland JH (1989) Classifier systems and genetic algorithms. *Artif Intell* 40(1):235–282.
46. Boyd S, Vandenberghe L (2004) *Convex Optimization* (Cambridge Univ Press, Cambridge, UK).
47. Saldarriaga J, Berger JD (2002) Flagellar motion in paramecium. Available at www.zoology.ubc.ca/courses/bio332/flagellar_motion.htm. Accessed January 26, 2015.
48. Rozvany GI, Olhoff N (2000) *Topology Optimization of Structures and Composite Continua* (Springer, Dordrecht, The Netherlands), Vol. 7.
49. Lum GZ, Teo TJ, Yeo SH, Yang G, Sitti M (2015) Structural optimization for flexure-based parallel mechanisms–Towards achieving optimal dynamic and stiffness properties. *Precis Eng* 42:195–207.
50. Shields AR, et al. (2010) Biomimetic cilia arrays generate simultaneous pumping and mixing regimes. *Proc Natl Acad Sci USA* 107(36):15670–15675.
51. van Oosten CL, Bastiaansen CW, Broer DJ (2009) Printed artificial cilia from liquid-crystal network actuators modularly driven by light. *Nat Mater* 8(8):677–682.
52. Vilfan M, et al. (2010) Self-assembled artificial cilia. *Proc Natl Acad Sci USA* 107(5): 1844–1847.
53. Zhang D, et al. (2014) A bio-inspired inner-motile photocatalyst film: A magnetically actuated artificial cilia photocatalyst. *Nanoscale* 6(10):5516–5525.
54. Kiral E, Eringen AC (1990) *Constitutive Equations of Non-linear Electromagnetic Elastic Crystals* (Springer, New York).
55. Diller E, Giltinan J, Lum GZ, Ye Z, Sitti M (2016) Six-degree-of-freedom magnetic actuation for wireless microrobotics. *Int J Robot Res* 35(1-3):114–128.